Annals of Case Reports
Najem H, et al. Ann Case Rep: 9: 101607
www.doi.org/10.29011/2574-7754.101607
www.gavinpublishers.com

OPEN ACCESS

GAVIN PUBLISHERS

Research Article

Prohibitin Expression in Antigen-Presenting Cells: Implications for Inciting Trigger in CNS IgG4-Related Disease

Hinda Najem[1,2#], Victor A Arrieta[1,2#], Joseph Duffy[1,2#], Shashwat Tripathi[1,2], Markella Zannikou[1], Silpol Dhiantravan[1,2], Jason Miska[1,2], Kathleen McCortney[1,2,3], Alicia Steffens[1,2,3], Jordain Walshon[1,2], Catalina Lee Chang[1,2], Nader S Dahdaleh[1], Adam M Sonabend[1,2], Zachary Smith[1,2], Craig M Horbinski[1,2,3], James Chandler[1,2], Amy B Heimberger[1,2*], Irina V Balyasnikova[1,2*]

[1]Department of Neurological Surgery, Feinberg School of Medicine, Northwestern University, Chicago, IL, USA

[2]Northwestern Medicine Malnati Brain Tumor Institute of the Lurie Comprehensive Cancer Center, Feinberg School of Medicine, Northwestern University, Chicago, IL, USA

[3]Department of Pathology, Feinberg School of Medicine, Northwestern University, Chicago, IL, USA

[#]All three primary authors contributed equally to the data.

[*]**Corresponding authors:** Amy B Heimberger, Department of Neurological Surgery, Feinberg School of Medicine, Northwestern University, Chicago, IL, USA.

Irina V Balyasnikova, Department of Neurological Surgery, Feinberg School of Medicine, Northwestern University, Chicago, IL, USA.

Citation: Najem H, Arrieta VA, Duffy J, Tripathi S, Zannikou M, et al. (2024) Prohibitin Expression in Antigen-Presenting Cells: Implications for Inciting Trigger in CNS IgG4-Related Disease. Ann Case Report 9: 1607. DOI: 10.29011/2574-7754.101607

Received: 19 January 2024; **Accepted:** 23 January 2024; **Published:** 25 January 2024

Abstract

Immunoglobulin G4-related disease (IgG4-RD) is a rare autoimmune disorder with an unknown etiology. Using orthogonal immune profiling and automated sequential multiplexing, we found an enhanced frequency of activated circulating B cells, antigen-presenting myeloid cells in peripheral blood, and a distinct distribution of immune cells within the CNS lesions. Prohibitin-expressing CD138+ plasma B cells and CD11c+ dendritic cells have been found interacting with T cells resulting in immune cell activation within the lesion. The data implicate prohibitin as a potential triggering antigen in the pathogenesis of IgG4-RD and shed light on the cellular dynamics and interactions driving IgG4-RD in the central nervous system, emphasizing the need for further studies corroborating these findings.

Keywords: IgG4-Related Disease; Prohibitin; Antigen Presentation; Plasma Cells; T Cells; Myeloid Cells; Immune Activation

Introduction

Immunoglobulin G4-related disease (IgG4-RD) is a relatively rare autoimmune condition with the potential to affect almost any organ in the body. Predominantly observed in older males, it presents as fibrosis combined with dense lymphoplasmacytic infiltration, including abundant IgG4+ CD138+ plasma cells and a distinctive increased IgG4: IgG ratio exceeding 40% [1]. Key mediators of the inflammatory response in IgG4-RD lesions are B cells and CD4+ T cells. Notably, the frequency of CD4+ cytotoxic T cells has been linked to both serum IgG4 levels and the overall lesion count [2]. These CD4 T cells support the differentiation of naïve B cells into plasmablasts, mediate the expansion of CD138+ plasmablasts, and induce the IgG4 class switch [2]. Additionally, emerging studies hint at the involvement of CD8+ memory T cells in the pathogenesis of the disease [3]. While a better understanding of the systemic manifestations of IgG4-RD is underway, its implications within the central nervous system (CNS) remain relatively unclear. This study provides novel insights into the clinical manifestations, development, and progression of IgG4-RD within the CNS.

Clinical Summary of Human Subjects' Cases

A 66-year-old male presented with a complex and progressive constellation of symptoms over a period of 5 years, including hypogonadism, episodic weakness, syncope, persistent fatigue, dry skin, diminished vision, and mild frontal headaches. The sudden onset of diplopia prompted a magnetic resonance imaging (MRI) evaluation. The MRI revealed a 1.8 cm bilobed lesion with homogenous gadolinium enhancement situated in the suprasellar region abutting the optic chiasm (Figure 1, T1 MRI). The enhancing mass extended from the floor of the Sella to the suprasellar cistern, causing an upward displacement of the optic chiasm and effacing its inferior margin. There was no involvement of the cavernous sinuses. The endocrine evaluation demonstrated normal parameters for serum sodium, prolactin (18.7ng/ml), thyroid-stimulating hormone (TSH; 3.26mIU/ml), stimulating follicle hormone/luteinizing hormone (FSH/LH; 0.3), and growth hormone (GH; <0.1ng/mL). A visual field examination revealed a field defect. Notably, a PET scan highlighted numerous hypermetabolic lymph nodes. The patient's serum IgG4 level was elevated to 105.4mg/dl, while other IgG subclasses remained within the normal range. An abdominal CT scan presented no abnormalities in the pancreas or other organ systems. The patient received preoperative steroids and subsequently underwent transsphenoidal biopsy of the lesion. Histology showed extensive infiltration of the pituitary tissue by mature CD138+ plasma cells and CD3+ T cells, with relatively few scattered CD20+ B cells. The kappa to lambda ratio was approximately 2:1, and nearly 40% of all IgG-positive plasma cells tested positive for IgG4 (Figure 1A-I). Cumulatively, these features were consistent with a diagnosis of IgG4-RD. Following surgery, steroid treatment, and hormone replacement for panhypopituitarism significantly alleviated the patient's symptoms. He subsequently regained an optimal state of health. Periodic follow-up over three years post-diagnosis showed no evidence of disease progression.

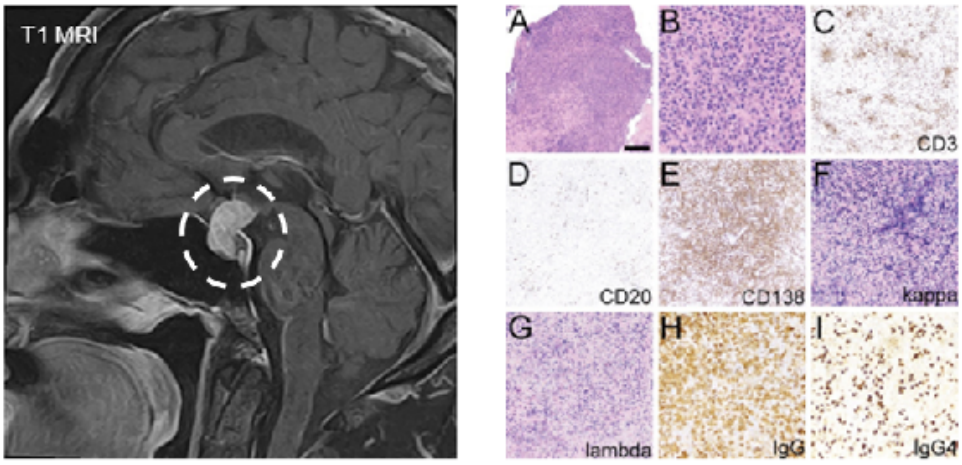

Figure 1: T1 weighted MRI scan showing the space-occupying lesion within the Sella of the IgG4-RD patient involving the pituitary (highlighted by a dashed circle). (A, B) Hematoxylin and eosin staining at 2.5x and 10x magnification respectively. (C-I) Immunohistochemistry diagnostic staining of the pituitary lesion for (C) CD3, (D) CD20, (E) CD138, (F) Kappa, (G) Lambda, (H) total IgG, and (I) IgG4. Magnification at 10x.

While the second case has been previously reported, it lacked an in-depth immunological characterization [4]. Briefly, the subject was a 48-year-old female who presented with a two-month history of progressive back pain accompanied by right leg radiculopathy. Clinically, she displayed no neurological deficits. A spine MRI revealed an extradural mass localized at the level of L2-L3 vertebrae, extending beyond the right neural foramen. A comprehensive chest and abdominopelvic CT scan found no other discernible lesions. A subsequent excisional biopsy of the spinal lesion demonstrated similar histopathology to the first case, including robust plasma cell infiltration. Following a treatment regimen with dexamethasone, the patient reported no symptoms during a one-year follow-up and exhibited no evidence of recurrent disease.

Materials and Methods

Study Approval

This study and analysis were conducted under a Northwestern Medicine IRB-approved protocol STU00211542. Blood and surgically resected formalin-fixed and paraffin-embedded tissue from two cases of IgG4 disease (localized to the pituitary and spine) were collected by the Northwestern Nervous System Tumor Bank (STU00095863) after patients provided informed consent.

Purification of PBMCs

PBMCs were isolated by density gradient using Lymphocyte Separation Media (Corning). Following the centrifugation step, PBMCs were collected and processed.

Cytek Spectrum Profiling

Then, CD8 T cells were resuspended in a low volume of pre-warmed thawing cell culture media and placed at 37ºC in a CO2 incubator. Cells were stimulated (100x stimulation cocktail) for 2h in complete RPMI. First, CD8 T cells were stained for viability and surface markers (Alexa Fluor 700-conjugated anti-human CD8 (SK1; Biolegend), then permeabilized with perm-fix (company), and stained for intracellular markers. PBMCs were stained for 30 min on ice with allophycocyanin (APC)-conjugated anti-human Granzyme-B (San Diego, CA; Biolegend), R-phycoerythrin (PE)-conjugated anti-human CD120b (TNFR) (3G7A02; Biolegend), and peridinin chlorophyll protein (PerCP)-Cy5.5-conjugated anti-human CD137 (4-1BB) (309813; Biolegend) and R-phycoerythrin-Cyanine 7 (PE/CY7)-conjugated anti-human IFN-γ (4S.B3; Biolegend). After incubation with antibodies, cells were washed twice with FACS buffer by centrifugation at 300 × g for 10 min at 4°C and analyzed with a BD FACSCalibur benchtop flow cytometer. The data were analyzed using FlowJo 7.6 software (FlowJo, LLC). Percentages of CD8+ T cells and CD8+ T lymphocytes expressing different markers presented as mean ± SEM (n = 3).

RNA Extraction and Library Preparation

Total RNA was extracted from samples stored in TRIzol, as described by the manufacturer (Thermo Fisher Scientific). The quality and concentration of the extracted RNA were estimated in a Nanodrop ND-1000 spectrophotometer (Thermo Scientific). The mRNA is randomly fragmented with a fragmentation buffer for further library construction. cDNA was synthesized, followed by adenylation of the 3' ends of DNA fragments was performed before ligating the NEBNext Adaptor with hairpin loop structure to prepare for hybridization. The library was obtained by PCR amplification and purification of PCR products using AMPure XP beads. The quality of the library was assessed with Qubit2.0 and detected the insert size by Agilent 2100. Libraries were fed into Illumina machines after pooling them according to activity and expected data volume.

RNA-seq Analysis

Raw image data file from high-throughput sequencing was transformed into sequence reads by CASAVA base recognition (base calling). Raw data were stored in FASTQ format files containing reads sequence and corresponding base quality. The ectopic follicle-like formations content was assessed along sequence reads. Next, data were filtered and cleaned, followed by performing the alignment of reads to the human genome employing STAR. Gene expression was estimated by the abundance of transcripts that mapped to the genome.

For CIBERSORT analysis [5], the PBMCs were collected from three subjects: a healthy donor, a patient diagnosed with pituitary adenoma, and a patient with IgG4-RD. Each source provided a single biological replicate, and from each of these, three technical replicates were generated to ensure reproducibility. Gene expression profiling of the PBMCs was conducted using standardized protocols, focusing on a signature matrix derived from barcode genetic expression profiles encompassing 547 genes. Each technical replicate's resulting gene expression datasets were subsequently uploaded to the CIBERSORT web portal (http://cibersort.stanford.edu/). For the analysis, the number of permutations was set at 1000. Using CIBERSORT, the representation of 22 distinct immune cell types was quantified within each PBMC sample. Key metrics, including the p-value, Pearson's correlation coefficient, and root mean squared error (RMSE), were determined for each sample. Results yielding a p-value of ≤ 0.05 were considered statistically significant.

Multiplexing Fluorescence Staining

The multiplex panel included the following unconjugated antibodies: CD31 (endothelial cells; Abcam EPR3131), CD4 (T helper cells; Abcam EPR17259), CD8 (cytotoxic T cells; Leica 4B11), CD45RO (memory T cells; US Biological SPM125),

CD19 (B cells; Abcam EPR5906), CD20 (B cells; Dako Agilent L26), CD27 (memory B cells; Abcam EPR8569), CD138 (Plasma B cells; Dako Agilent MI15), CD11c (antigen presenting cells; Abcam EP1347Y), CD205 (Dendritic cells; Abcam EPR5233), CD68 (pan monocyte/macrophage; Dako Agilent PG-M1), CD163 (macrophage scavenger receptor; Abcam EPR19518), Granzyme B (machinery for cell killing; Santa Cruz 2C5), IFN-γ (Pro-inflammatory cytokine; Abcam IFNG/466), TNF-α (Pro-inflammatory cytokine; Abcam), FOXP3 (T regulatory cells; Cell signaling tech D2W8E), HLA-DR (MHC class 2; Abcam TAL 1B5), PD-1 (Immune checkpoint inhibitor; Abcam EPR4877(2)), PD-L1 (Immune checkpoint inhibitor; GenomeMe IHC411), p-LCK (T cell activation marker; Novus Bio 755103), Prohibitin (Pro-inflammatory agent, Abcam EP2803Y). All antibodies were validated using conventional immunohistochemistry and/or immunofluorescence (IF) staining, in conjunction with the corresponding fluorophore and the spectral 4',6-diamidino-2-pheynlindole (DAPI; Thermo Fisher Scientific) counterstain. For optimal concentration and the best signal/noise ratio, all antibodies were tested at three different dilutions, starting with the manufacturer-recommended dilution (MRD), then MRD/2 and MRD/4. Secondary Alexa fluorophore 555 (ThermoFisher Scientific) and Alexa fluorophore 647 (ThermoFisher Scientific) were used at 1/200 and 1/400 dilutions, respectively. The optimizations and full runs of the multiplex panel were executed using the sequential IF (seqIF™) methodology integrated into the Lunaphore COMET™ platform (characterization 2 and 3 protocols, and seqIF™ protocols, respectively) [6]. The staining can be performed at a maximum of 4 tissue slides simultaneously following automated cycles of 2 antibodies' staining at a time, followed by imaging and elution, where no sample manipulation is required. Image stacking and visualization were accessed immediately after concluding the staining procedure. Slides were automatically scanned using the Lunaphore COMET™ following the manual's instructions with a fluorescent high-power field scan (20x magnification microscope). The microscope captures the fluorescent signals (DAPI, TRITC, and Cy5) separately at the corresponding fluorophore wavelength, with preset exposure times. Then, these captures are stacked in one image (OME.TIFF) without disrupting the unique fluorescent spectral signature of the markers.

ELISA

The ELISA plate was coated with the prohibitin recombinant protein (Abcam) at 1 µg/ml in PBS and stored overnight at 4ºC. The next day, the protein-coated plate was washed and blocked with PBS containing 2% FBS. Plasma from 3 donors and two patients (NU1200 and NU1208) was titrated over the prohibitin plate and incubated for 1 h at room temperature with continuous shaking. After the wash with PBS-Tween20, mouse anti-IgG4 antibodies (Invitrogen) conjugated with horseradish peroxidase were applied at the dilution 1:1000 for 1 hour, washed, and detected with TMB-slow substrate (ThermoFisher Scientific). The developing reaction was stopped with 2N HCl, and the plate was read at OD450 using the Bio-Tek plate reader.

Results and Discussion

We analyzed formalin-fixed paraffin-embedded (FFPE) tissue samples from two distinct patient cases with IgG4-RD, one localized to the pituitary and the other to the spine. Alongside these, matched peripheral blood mononuclear cells (PBMCs) from the pituitary IgG4-RD case, a control sample from a pituitary adenoma, and samples from three healthy donors (HD) were immunophenotyped. Using spectral flow cytometry (Figure 2, Suppl. Figure 1) combined with CIBERSORT analysis (Figure 3), we found that peripheral CD19+ B cells of the IgG4-RD patient displayed an activated phenotype as indicated by the expression of HLA-DR and granzyme B (Figure 2A). Furthermore, the IgG4-RD patient's myeloid cells, identified as CD11b+ CD14+, suggested enhanced antigen presentation capacity, marked by an elevated HLA-DR expression (Figure 2B). While there was an absence of peripheral CD138+ plasma cells in the blood (Figure 3), these cells were abundant within the lesion itself (Figure 4). In the IgG4-RD patient, peripheral CD4+ T cells expressing PD-1 and effector CD8+ T cells with elevated granzyme B were detected in the IgG4-RD patient (Figure 2C). The significance of this observation was underscored by differential gene expression analysis from RNA-seq data revealing a fold change of 1.75 (p adj. value <0.001; (Suppl. Figure 2). Naïve T cells were mostly absent in the patient with IgG4-RD relative to healthy donors (Figure 2C). However, there was a marked increase in IFN-γ+ T cells (Figure 2C). Collectively, the findings from the comprehensive immunophenotypic analysis provide valuable insights into the systemic cellular dynamics and interactions in cases of IgG4-RD.

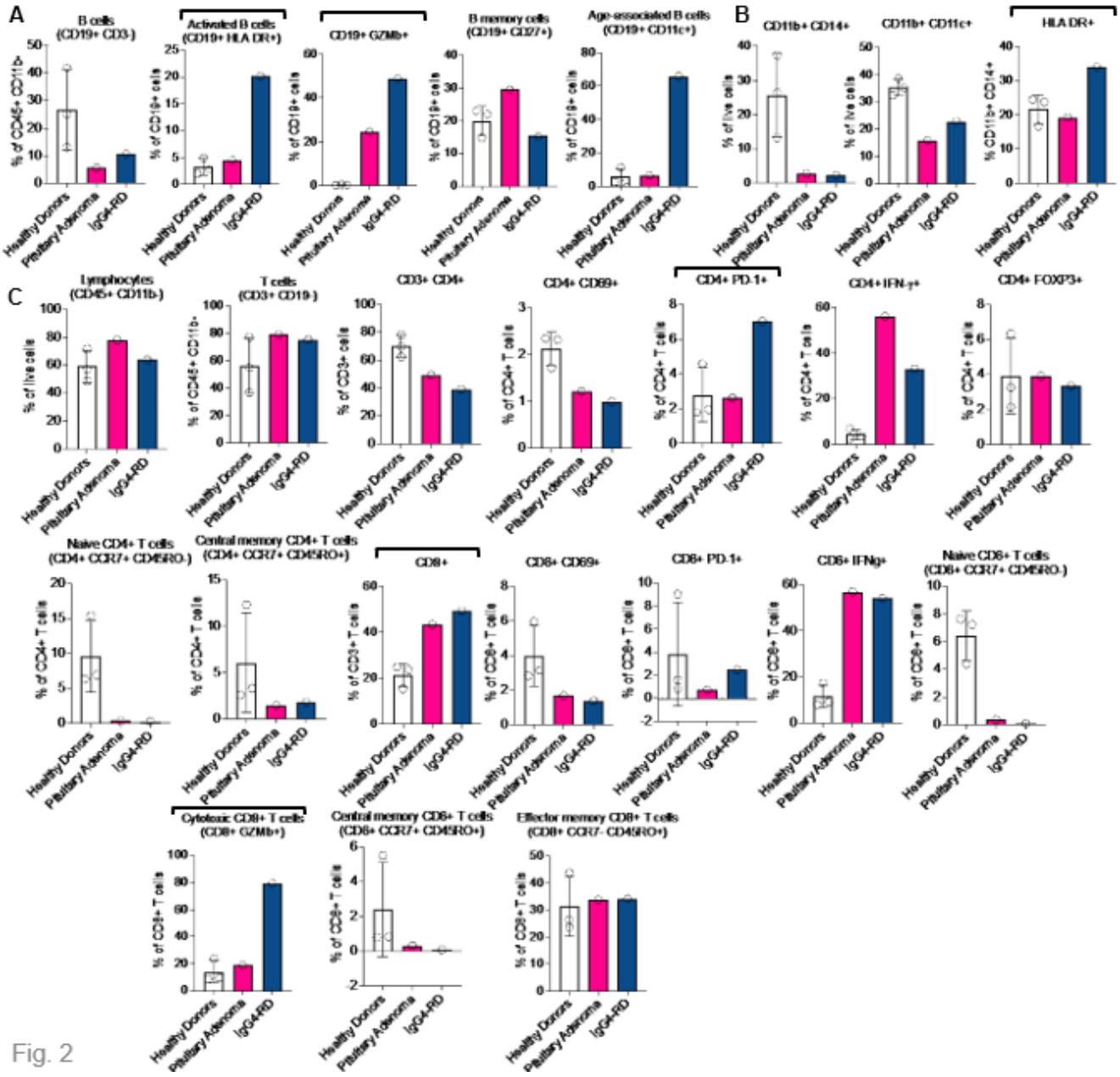

Fig. 2

Figure 2: Cytek Spectrum comprehensive immunophenotyping of PBMCs from healthy donors (n=3), a pituitary adenoma patient, and a patient with IgG4-RD. Bar plots showing the percentages of (A) B cells (CD19+CD3-), activated B cells (CD19+HLADR+), GZMb+CD19+ B cells, B memory cells (CD19+CD27+), and age-associated B cells (CD19+CD11c+); (B) Myeloid cells (CD11b+CD14+ and CD11b+CD11c+), and CD11b+CD14+HLA DR+ antigen-presenting cells; (C) lymphocytes (CD45+ CD11b-), T cells (CD3+ CD19-), CD4+ T cells, CD4+CD69+, PD-1+CD4+, and CD4+IFN-γ+ T cells, CD4+FOXP3+ T regulatory cells, Naïve CD4+ T cells, and Central memory CD4+ T cells (CD4+ CCR7+CD45RO+), CD8+ T cells, CD8+CD69+, CD8+PD-1+, and CD8+IFN-γ+ T cells, Naïve CD8+ T cells (CD8+CCR7+CD45RO-), granzyme+ (GZMb+) CD8+ cytotoxic T cell, Effector memory CD8+ T cells (CD8+CCR7-CD45RO+), and Central memory CD8+ T cells (CD8+CCR7+CD45RO+). Each point represents a sample and relevant changes are designated by top black brackets. Gating and additional details are provided in Supplementary Figure 1.

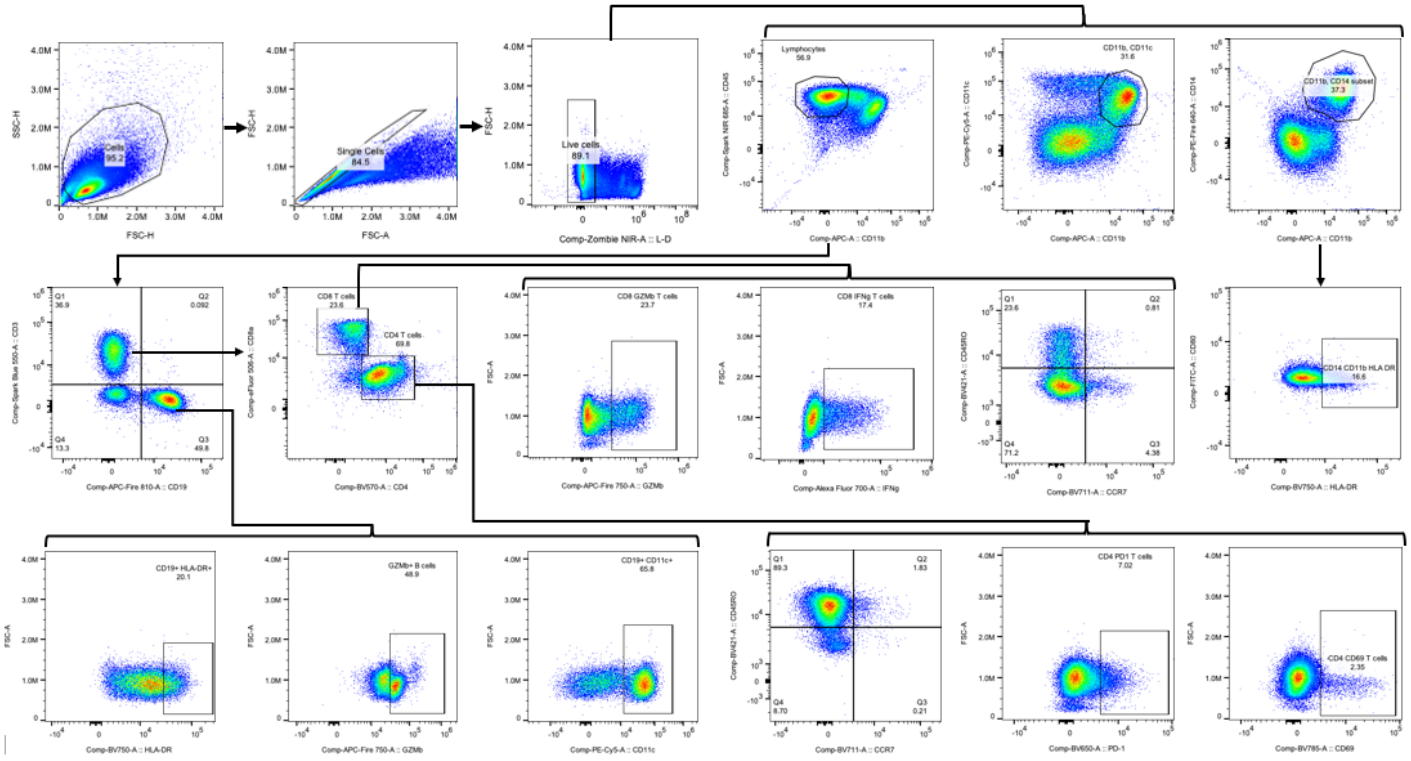

Supplementary Figure 1: Cytek spectrum gating strategy used to analyze the production of cytokines and the expression of surface markers in PBMCs from healthy donors, a pituitary adenoma patient, and a patient with IgG4-RD. Immune cells were gated based on SSC and FSC parameters followed by the exclusion of doublets. Next, live cells were gated based on low values of Zombie NIR fluorescence intensity. Subsequently, live cells were gated based on the expression of CD45+, CD11b+, CD11c+, and CD14+. Then, lymphocytes were gated based on CD45+ and CD11b- followed by gating employing CD3+ and CD19+ markers. IFN-g+, GZMb+, HLA-DR+, CD11c+, PD-1+, CD69+, CD45RO+, and CCR7+ were evaluated on CD3+ T cells and CD19+ B cells.

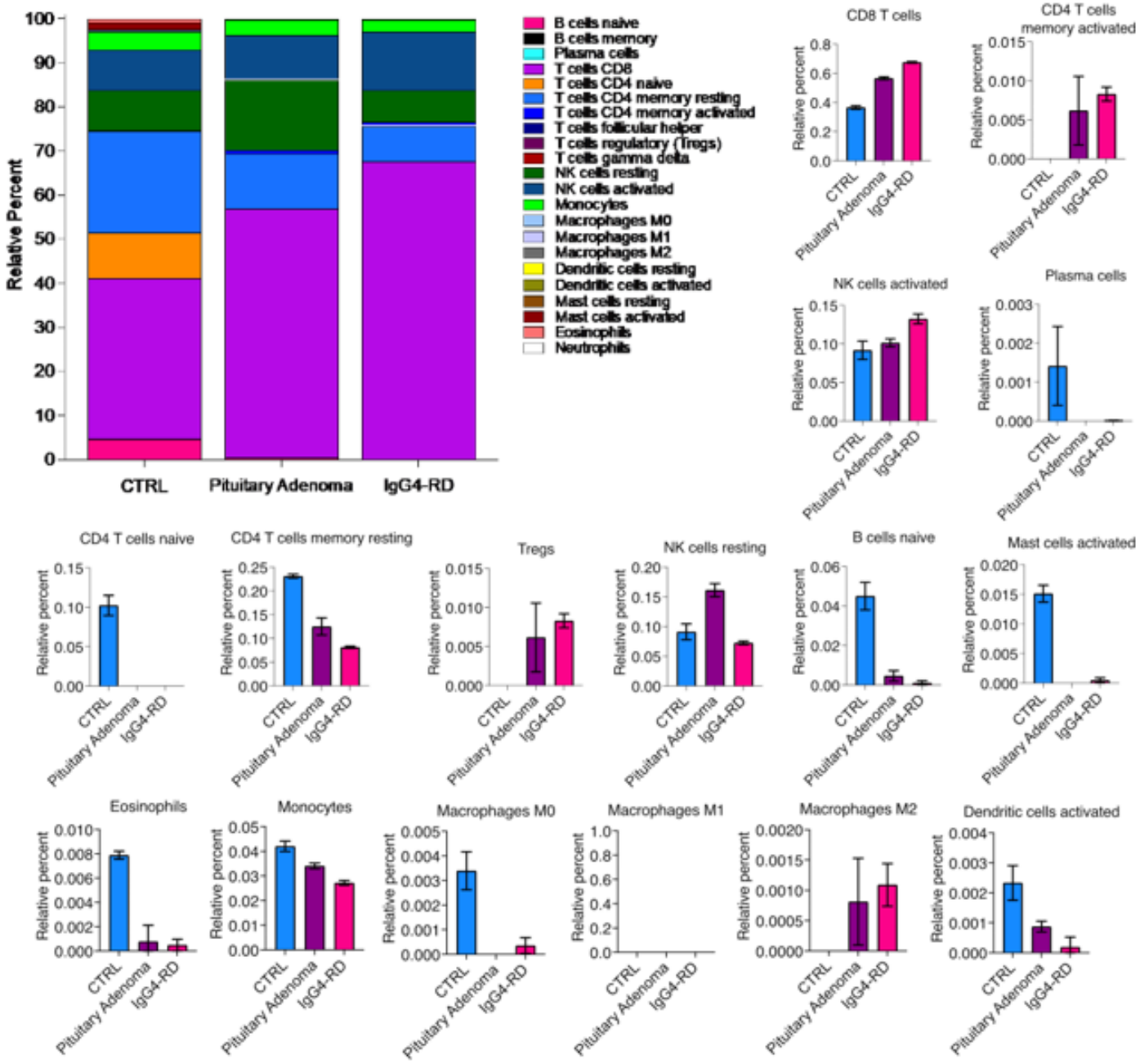

Figure 3: CIBERSORT analysis of PBMCs from a healthy donor, a pituitary adenoma patient, and a patient with IgG4-RD. Colored map showing the immune composition for each condition in technical triplicates, along with corresponding bar plots showing the relative percentage of CD8 T cells, memory-activated CD4 T cells, activated NK cells, plasma cells, CD4 T cells naïve, CD4 T cells memory resting, Tregs, NK cells resting, Mast cells activated, B cells naïve, Eosinophils, Monocytes, Macrophages M0, Macrophages M1, Macrophages M2, and Dendritic cells activated.

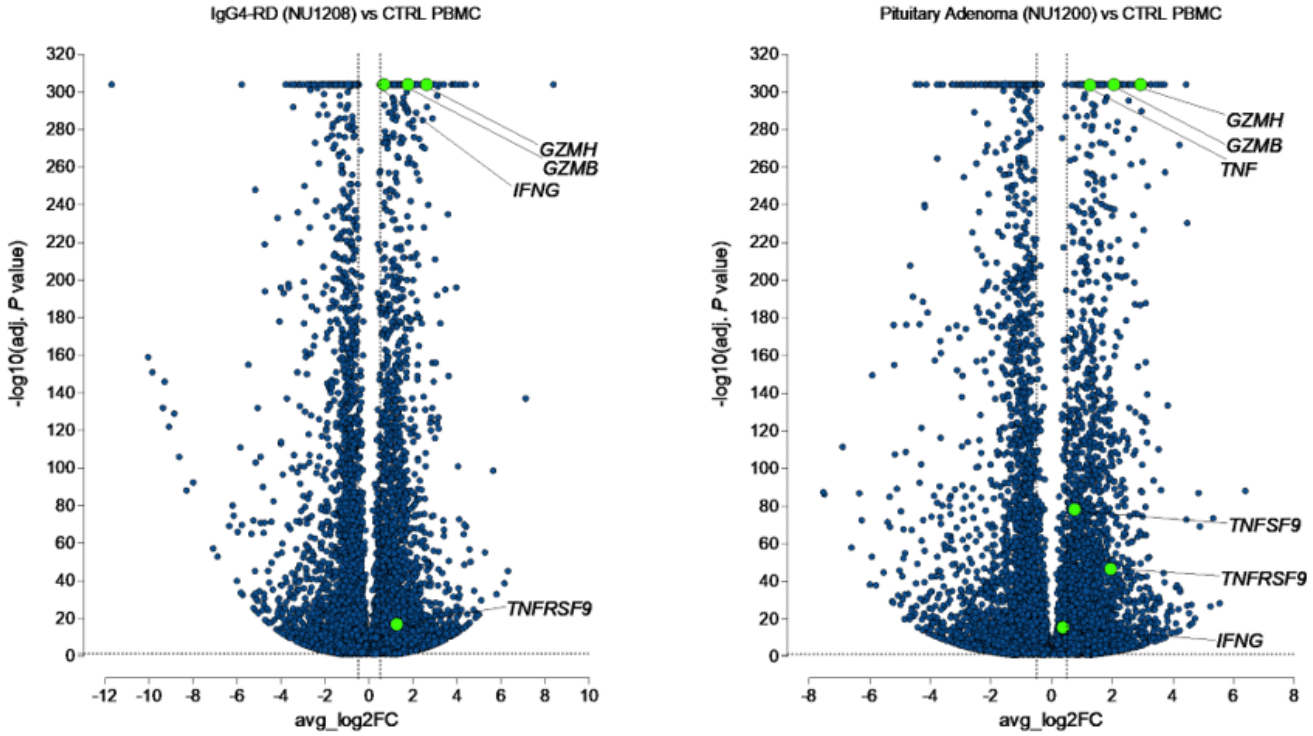

Supplementary Figure 2: Differential gene expression analysis of PBMCs from a healthy donor, a pituitary adenoma patient, and a patient with IgG4-RD. Volcano plots comparing PBMCs from a patient with IgG4-RD against PBMCs from a healthy donor (left) and PBMCs from a patient with pituitary adenoma against PBMCs from a healthy donor (right).

Previous research has demonstrated that the majority of IgG4-RD patients have circulating IgG4 antibodies targeting prohibitin [7]. Prohibitin has a variety of functions, including the activation of B cells through CD86 binding [8]. According to the Human Protein Atlas (https://www.proteinatlas.org/ENSG00000167085-PHB/brain), prohibitin is also expressed within the CNS. In keeping with prior research, we analyzed plasma samples from the pituitary IgG4-RD patient, the pituitary adenoma patient, and from healthy donors and found elevated anti-prohibitin antibodies in the case of IgG4-RD adenohypophysitis (Figure 4A).

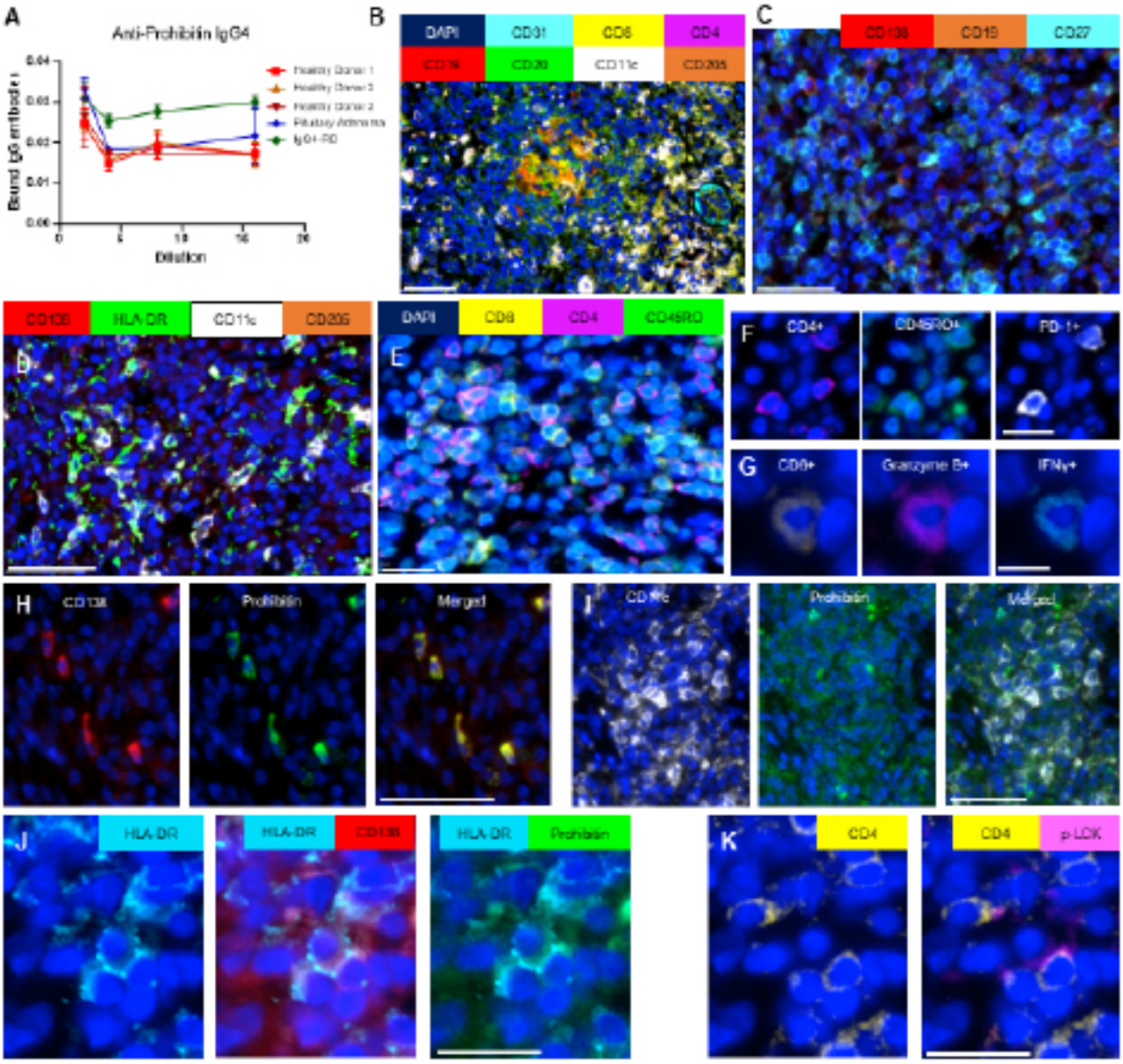

Figure 4: (A) ELISA anti-prohibitin antibody detection essay from the plasma of 3 healthy donors, pituitary adenoma (NU1200), and the pituitary IgG4-RD (NU1208) patient. (B-K) Multiplex imaging of the pituitary IgG4 lesion showing (B) CD20+ and CD19+ B cells forming follicular-like formations surrounded by CD8+, CD4+ T cells, CD11c+ myeloid cells, and CD11c+CD205+ dendritic cells (DCs). Scale bar: 50µm. (C) Plasma CD19+CD138+CD27+ cells and memory CD19+CD27+CD138- B cells within the IgG4 lesion. Scale bar: 50µm. (D) CD11c+CD205+HLA-DR+ DCs clustered near the plasma cells and memory B cells. Scale bar: 50µm. (E) Memory CD4+ T cells (CD4+CD45RO+) and cytotoxic memory T cells (CD8+CD45RO+). Scale bar 20µm. (F) PD1+CD4+ T cells and (G) CD8+ T cells expressing granzyme B and IFN-γ scattered throughout the IgG4 lesion. Scale bars at 20 µm and 10 µm, respectively. (H) Prohibitin is expressed in the cytoplasm of CD138+ plasma B cells and (I) within CD11c+ antigen-presenting cells. Scale bar: 50µm. (J) Serial multiplex images showing the expression of HLA-DR and prohibitin by CD138+ plasma cells in proximity with CD4+ T cell expressing (K) p-LCK at the interface between these cells. These interactions were found diffusely throughout the IgG4 lesions. Scale bars: 20µm.

For a deeper understanding, we conducted a multiplex immunofluorescence profiling on the pituitary and spinal IgG4-RD lesions to directly assess and characterize the immune reactivity directly within the lesions. The distribution of immune cells resembled that of an immune cluster interaction induced by an antigen with CD20+ and CD19+ B cells surrounded by CD8+, CD4+ T cells, CD11c+ myeloid cells, and CD11c+CD205+ dendritic cells (DCs) (Figure 4B). DCs are known to modulate B cell diversity, which may affect epitope spreading during autoimmunity [9]. Plasma CD19+CD138+CD27+ cells and memory CD19+CD27+CD138- B cells were diffusely distributed throughout the IgG4-RD lesions (Figure 4C). CD11c+CD205+HLA-DR+ DCs clustered around the follicle-like formations with plasma cells and memory B cells (Figure 4D). Memory CD4+ T cells (CD4+CD45RO+) and cytotoxic memory T cells (CD8+CD45RO+) were also found in these areas (Figure 4E). Additionally, CD45RO+ memory CD4+ T cells expressing PD-1 (Figure 4F) and CD8+ T cells expressing granzyme B and IFN-γ (Figure 4G) were occasionally found in the tissue.

TIGIT-expressing follicular helper CD4+ T cells are increased in the tertiary lymphoid organs of IgG4-RD patients [10]. However, our analysis showed that there was increased expression of PD-1 but not TIGIT on the CD4+ T cells in the PBMCs and within the CNS lesions (Figure 2C and 4F). In the spinal case of IgG4-RD, there were more CD4+ T cells (predominantly FoxP3+) relative to CD8+ T cells and CD163+ expressing myeloid cells. However, the most prevalent immune cell populations identified in the lesions were CD11c+CD205+HLA-DR+ DCs and CD138+ plasma B cells.

Multiplex imaging revealed the presence of prohibitin in both the pituitary and spine IgG4-RD lesions, particularly within the cytoplasm of CD138+ plasma B cells (Figure 4H) and DCs (Figure 4I). These immune cells may function as antigen-presenting cells given their expression of HLA-DR (a component of MHC II) and their direct contact with T cells (Figure 4J). These observations suggest that prohibitin-expressing HLA-DR+ antigen-presenting cells might be engaged in an immunological synapse with T cells, as indicated by the expression of p-LCK (Figure 4K). This supports the hypothesis that prohibitin might be a critical disease-triggering antigen.

The cumulative data suggests that either through epitope mimicry, inadvertent presentation of intracellular thymically-naïve antigens, and/or through alterations of the LAT signalosome [11], prohibitin may be antigenically processed by either the CD138+ B cell or the CD11c+ cells triggering the infiltration and activation of both T and B cell responses. Tregs and T helper cells could then further modulate the oligoclonal expansion of plasmablasts and the subsequent IgG class switching in B cells. The formation of the immune clusters in the lesion and the development of immunological memory can be attributed to active immunological antigen presentation within the IgG4-RD lesion, likely contributing to the pathogenesis of IgG4-RD. The expression of prohibitin in organs affected by IgG4-RD suggests its potential role as a triggering antigen both within and outside the CNS. Future studies should be directed at ascertaining if the antibodies present in the IgG4 lesion are specific to prohibitin, identifying the specific prohibitin peptide being presented by MHC, and defining the responding TCR.

Statistical analysis of the data

Statistical significance was evaluated in pairwise comparisons with control values using a One-way ANOVA test after confirmation of normal distributions with GraphPad Prism 8.0. All samples were quantified as means + SEM, and $P < 0.05$ was considered significant.

Conflict of Interest: ABH serves on the advisory board of Caris Life Sciences and the WCG Oncology Advisory Board and is supported by research grants from Alnylam and AbbVie. IVB holds patents on antibodies targeting IL13Ra2 and their applications in cancer and CAR T cells. The rest of the authors declare that the research was conducted in the absence of any commercial or financial relationships that could be construed as a potential conflict of interest.

Author Contributions: Experimental design: ABH, IVB. Methodology and execution: HN, VAA, JD, KM, IVB. Funding acquisition: ABH, IVB. Data analysis: HN, VAA, JD, MZ, KLK, ABH, IVB. Initial draft and writing: HN, VAA, JD, ABH, IVB. Manuscript review: All authors. All authors approved the final manuscript.

Funding: Support was provided by the Northwestern Medicine Malnati Brain Tumor Institute of the Lurie Cancer Center and NIH grants NS120547, CA120813, NS122395, NS106379, P30CA060553, and P50CA221747 and a gracious gift from the Stephen Coffman Foundation.

Acknowledgments: Special thanks to Bella Najem, BA in Fashion Design and Media, for her expertise in media and animated video generation. Histology services were provided by the Northwestern University Neurological Surgery Nervous System Tumor Bank. Clinical data collection was conducted by Kwok Ling Kam. We want to thank the Immunotherapy Assessment Core of the Robert H. Lurie Comprehensive Cancer Center for their support with phenotyping peripheral blood immune cells.

Data Availability Statement: The data used to support the findings of this study are available within this article.

References

1. Umehara H, Okazaki K, Masaki Y, Kawano M, Yamamoto M, et al. (2012) Comprehensive diagnostic criteria for IgG4-related disease (IgG4-RD), 2011. Mod Rheumatol 22(1):21-30.
2. Mattoo H, Stone JH, Pillai S (2017) Clonally expanded cytotoxic CD4(+) T cells and the pathogenesis of IgG4-related disease. Autoimmunity 50(1):19-24.
3. Friedrich M, Kehl N, Engelke N, Kraus J, Lindner K, et al. (2021) Intrathecal activation of CD8(+) memory T cells in IgG4-related disease of the brain parenchyma. EMBO Mol Med 13(8):e13953.
4. Winkel M, Lawton CD, Sanusi OR, Horbinski CM, Dahdaleh NS, Smith ZA (2018) Neuro-surgical considerations for treating IgG4-related disease with rare spinal epidural compression. Surg Neurol Int 9:209.
5. Newman AM, Liu CL, Green MR, Gentles AJ, Feng W, et al. (2015) Robust enumeration of cell subsets from tissue expression profiles. Nat Methods 12(5):453-7.
6. Rivest F, Eroglu D, Pelz B, Kowal J, Kehren A, et al. (2023) Fully Automated Sequential Immunofluorescence (seqIF) for Hyperplex Spatial Proteomics. bioRxiv.
7. Du H, Shi L, Chen P, Yang W, Xun Y, et al. (2015) Prohibitin Is Involved in Patients with IgG4 Related Disease. PLoS One 10(5):e0125331.
8. Lucas CR, Cordero-Nieves HM, Erbe RS, McAlees JW, Bhatia S, et al. (2013) Prohibitins and the cytoplasmic domain of CD86 cooperate to mediate CD86 signaling in B lymphocytes. J Immunol. 190(2):723-36.
9. van der Poel CE, Bajic G, Macaulay CW, van den Broek T, Ellson CD, et al. (2019) Follicular Dendritic Cells Modulate Germinal Center B Cell Diversity through FcγRIIB. Cell Reports 29(9):2745-55.e4.
10. Akiyama M, Kaneko Y (2021) Recent Advances in Understanding the Role of TIGIT+ Follicular Helper T Cells in IgG4-Related Disease. Immuno 1(4):380-90.
11. Joachim A, Aussel R, Gélard L, Zhang F, Mori D, et al. (2023) Defective LAT signalosome pathology in mice mimics human IgG4-related disease at single-cell level. Journal of Experimental Medicine 220(11).